COMPUTER METHODS IN APPLIED MECHANICS AND ENGINEERING 87 (1991) 363–384
NORTH-HOLLAND

TIME-ACCURATE INCOMPRESSIBLE FLOW COMPUTATIONS WITH QUADRILATERAL VELOCITY–PRESSURE ELEMENTS*

T.E. TEZDUYAR, S. MITTAL and R. SHIH
Department of Aerospace Engineering and Mechanics, and Minnesota Supercomputer Institute, University of Minnesota, Minneapolis, MN 55455, USA

Received 23 April 1990

Quadrilateral velocity–pressure elements with constant and linear pressure interpolations are examined in the context of time-accurate finite element computation of unsteady incompressible flows. These elements involve streamline–upwind/Petrov–Galerkin stabilization and are implemented in conjunction with the one-step and multi-step temporal integration of the Navier–Stokes equations. The two test cases chosen for the performance evaluation of the formulations are the standing vortex problem and flow past a circular cylinder at Reynolds number 100.

1. Introduction

In this paper, we examine, in the context of time-accurate finite element computation of unsteady incompressible flows, three of the quadrilateral velocity–pressure elements with constant and linear pressure interpolations. The elements covered in this study are Q1P0 (bilinear velocity/constant pressure), Q2P1 (biquadratic velocity/linear pressure) and pQ2P1 ('pseudo' biquadratic velocity/linear pressure). These elements involve streamline–upwind/Petrov–Galerkin (SUPG) stabilization [1, 2] to prevent the spurious oscillations that might appear in the presence of dominant advective terms. We implemented these elements by generalizing the one-step formulation presented in [1] for the Q1P0 element, and also by using the multi-step formulation presented in [2].

In the one-step (T1) formulation, the equation system for the velocity and pressure can be solved either implicitly or explicitly. In implicit computations the unknowns are reordered in such a way that the unknown velocities in each element appear before the unknown pressures. The SUPG supplement to the weighting function is applied to all terms in the momentum equation. Therefore, in explicit computations the coefficient matrix of the pressure equation is generally not symmetric except for the Q1P0 element.

The T6 formulation [2] is an extension of the T3 formulation [2]. The T3 formulation is a three-step operator splitting scheme in which the pressure and the viscous terms are treated implicitly in the first and third steps, while the advective terms are treated implicitly in the second step. This type of splitting is a special case of the θ-scheme presented in [3]. In the T6 formulation, each step of the T3 formulation is subdivided into two-steps to isolate the

*This research was sponsored by NASA-Johnson Space Center under grant NAG 9-449 and by NSF under grant MSM-8796352.

advective terms, and the SUPG supplement is applied only to the sub-steps involving the advective terms.

We consider two numerical tests: the standing vortex problem [4], and flow past a circular cylinder at Re = 100. The standing vortex problem is used to determine the level of numerical dissipation involved in a numerical solution technique. The cylinder problem has been studied by several researchers in the past (see for example [5–7]) and has become a benchmark problem [2]. Our investigations of the cylinder problem are based on the temporally periodic solutions; therefore for each element type we try to reach the periodic solution as quickly and efficiently as possible. For this purpose, we use the periodic solution obtained with the Q2P1/T6 formulation as initial condition for the other formulations.

2. The governing equations

Let Ω and $(0, T)$ denote the spatial and temporal domains with x and t representing the coordinates associated with Ω and $(0, T)$, respectively. We consider the following velocity–pressure formulation of the incompressible Navier–Stokes equations:

$$\rho\left(\frac{\partial u}{\partial t} + u \cdot \nabla u\right) - \nabla \cdot \sigma = 0 \quad \text{on } \Omega \times (0, T), \tag{1}$$

$$\nabla \cdot u = 0 \quad \text{on } \Omega \times (0, T), \tag{2}$$

where ρ and u are the density and velocity, and σ is the stress tensor given as

$$\sigma = -p\mathbf{I} + 2\mu\varepsilon(u) \tag{3}$$

with

$$\varepsilon(u) = \tfrac{1}{2}(\nabla u + (\nabla u)^t). \tag{4}$$

Here p and μ represent the pressure and viscosity while $\mathbf{I}$ denotes the identity tensor. Both the Dirichlet and Neumann type boundary conditions are taken into account as shown below:

$$u = g \quad \text{on } \Gamma_g, \tag{5}$$

$$n \cdot \sigma = h \quad \text{on } \Gamma_h, \tag{6}$$

where Γ_g and Γ_h are complementary subsets of the boundary Γ.

3. Spatial and temporal discretizations

Let $\mathscr{E}$ denote the set of elements resulting from the finite element discretization of the computational domain Ω into subdomains Ω^e, $e = 1, 2, \ldots, n_{el}$, where n_{el} is the number of elements. We associate to $\mathscr{E}$ the finite dimensional Sobolev spaces H^{1h} and H^{0h}. The trial and test function spaces are given as

$$S_u^h = \{u^h \mid u^h \in (H^{1h})^{n_{sd}},\ u^h = g^h \text{ on } \Gamma_g\}\ , \tag{7}$$

$$V_u^h = \{w^h \mid w^h \in (H^{1h})^{n_{sd}},\ w^h = 0 \text{ on } \Gamma_g\}\ , \tag{8}$$

$$S_p^h = V_p^h = \{q \mid q \in H^{0h}\}\ , \tag{9}$$

where n_{sd} is the number of space dimensions.

The T1 formulation employed in this work is essentially the same as the one used in [1]: Find $u^h \in S_u^h$ and $p^h \in S_p^h$, such that

$$\begin{aligned}
&\int_\Omega w^h \cdot \rho\left(\frac{\partial u^h}{\partial t} + u^h \cdot \nabla u^h\right) d\Omega + \int_\Omega \varepsilon(w^h) : \sigma^h \, d\Omega \\
&\quad + \sum_{e=1}^{n_{el}} \int_{\Omega^e} \delta^h \cdot \left[\rho\left(\frac{\partial u^h}{\partial t} + u^h \cdot \nabla u^h\right) - \nabla \cdot \sigma^h\right] d\Omega \\
&\quad + \int_\Omega q^h \nabla \cdot u^h \, d\Omega = \int_{\Gamma_h} w^h \cdot h^h \, d\Gamma \quad \forall w^h \in V_u^h \quad \forall q^h \in V_p^h\ .
\end{aligned} \tag{10}$$

Here δ^h is the streamline–upwind/Petrov–Galerkin (SUPG) supplement, at the element interiors, to the weighting function w^h [8].

The semi-discrete equations corresponding to (10) can be written as follows:

$$\tilde{M}a + \tilde{N}(v) + \tilde{K}v - \tilde{G}p = \tilde{F}\ , \tag{11}$$

$$G^t v = E\ , \tag{12}$$

where v is the vector of unknown nodal values of u^h, a is the time derivative of v, and p is the vector of nodal values of p^h. The matrices $\tilde{M}$, $\tilde{N}$, $\tilde{K}$ and $\tilde{G}$ are derived, respectively, from the time-dependent, advective, viscous and pressure terms. The vector $\tilde{F}$ is due to the Dirichlet and Neumann type boundary conditions (i.e., the g and h terms in (5) and (6)), whereas the vector E is due to the Dirichlet type boundary condition. All arrays with a superposed tilde can be decomposed into their Galerkin and SUPG parts:

$$\tilde{M} = M + M_\delta\ , \tag{13}$$

$$\tilde{N} = N + N_\delta\ , \tag{14}$$

$$\tilde{K} = K + K_\delta\ , \tag{15}$$

$$\tilde{G} = G + G_\delta\ , \tag{16}$$

$$\tilde{F} = F + F_\delta\ , \tag{17}$$

where the subscript δ identifies the SUPG contribution.

REMARK 1. The equation systems (11) and (12) can be solved implicitly by reordering the unknowns in such a way that the unknown velocities appear before the unknown pressures in each element; we define this as the consistent-reordered (CR) system. In such cases we perform 2 iterations per time step.

REMARK 2. The equation systems (11) and (12) can also be solved by treating the velocity explicitly in the momentum equation. The way the Q1P0 element is used in [2] leads to a symmetric coefficient matrix for pressure. All explicit T1 computations presented in this paper are based on such a symmetric system and the results are obtained with 2 iterations per time step.

The T6 formulation is described as follows:

1. Find $\tilde{u}^h_{n+\theta} \in (S^h_u)_{n+\theta}$ such that

$$\int_\Omega w^h \cdot \rho\left[\frac{\tilde{u}^h_{n+\theta} - u^h_n}{\theta\,\Delta t} + u^h_n \cdot \nabla u^h_n\right] d\Omega + \sum_{e=1}^{n_{el}} \int_{\Omega^e} \delta^h \cdot \left[\rho\left(\frac{\tilde{u}^h_{n+\theta} - u^h_n}{\theta\,\Delta t} + u^h_n \cdot \nabla u^h_n\right)\right] d\Omega = 0 \quad \forall w^h \in V^h_u . \tag{18}$$

2. Find $u^h_{n+\theta} \in (S^h_u)_{n+\theta}$ and $p^h_{n+\theta} \in S^h_p$ such that

$$\int_\Omega w^h \cdot \rho\,\frac{u^h_{n+\theta} - \tilde{u}^h_{n+\theta}}{\theta\,\Delta t}\, d\Omega + \int_\Omega \varepsilon(w^h) : \sigma^h_{n+\theta}\, d\Omega + \int_\Omega q^h\, \nabla \cdot u^h_{n+\theta}\, d\Omega = \int_{\Gamma_h} w^h \cdot h^h_{n+\theta} \quad \forall w^h \in V^h_u \quad \forall q^h \in V^h_p . \tag{19}$$

3. Find $\tilde{u}^h_{n+1-\theta} \in (S^h_u)_{n+1-\theta}$ such that

$$\int_\Omega w^h \cdot \rho\,\frac{\tilde{u}^h_{n+1-\theta} - u^h_{n+\theta}}{(1-2\theta)\,\Delta t}\, d\Omega + \int_\Omega \varepsilon(w^h) : \sigma^h_{n+\theta}\, d\Omega = \int_{\Gamma_h} w^h \cdot h^h_{n+\theta}\, d\Gamma \quad \forall w^h \in V^h_u . \tag{20}$$

4. Find $u^h_{n+1-\theta} \in (S^h_u)_{n+1-\theta}$ such that

$$\int_\Omega w^h \cdot \rho\left[\frac{u^h_{n+1-\theta} - \tilde{u}^h_{n+1-\theta}}{(1-2\theta)\,\Delta t} + u^h_{n+1-\theta} \cdot \nabla u^h_{n+1-\theta}\right] d\Omega + \sum_{e=1}^{n_{el}} \int_{\Omega^e} \delta^h \cdot \left[\rho\left(\frac{u^h_{n+1-\theta} - \tilde{u}^h_{n+1-\theta}}{(1-2\theta)\,\Delta t} + u^h_{n+1-\theta} \cdot \nabla u^h_{n+1-\theta}\right)\right] d\Omega = 0 \quad \forall w^h \in V^h_u . \tag{21}$$

5. Find $\tilde{u}^h_{n+1} \in (S^h_u)_{n+1}$ such that

$$\int_\Omega w^h \cdot \rho\left[\frac{\tilde{u}^h_{n+1} - u^h_{n+1-\theta}}{\theta\,\Delta t} + u^h_{n+1-\theta}\cdot\nabla u^h_{n+1-\theta}\right] d\Omega$$
$$+ \sum_{e=1}^{n_{el}} \int_{\Omega^e} \delta^h \cdot \left[\rho\left(\frac{\tilde{u}^h_{n+1} - u^h_{n+1-\theta}}{\theta\,\Delta t} + u^h_{n+1-\theta}\cdot\nabla u^h_{n+1-\theta}\right)\right] d\Omega = 0 \quad \forall w^h \in V^h_u . \tag{22}$$

6. Find $u^h_{n+1} \in (S^h_u)_{n+1}$ and $p^h_{n+1} \in S^h_p$ such that

$$\int_\Omega w^h \cdot \rho\,\frac{u^h_{n+1} - \tilde{u}^h_{n+1}}{\theta\,\Delta t}\,d\Omega + \int_\Omega \varepsilon(w^h) : \sigma^h_{n+1}\,d\Omega + \int_\Omega q^h \nabla\cdot u^h_{n+1}\,d\Omega$$
$$= \int_{\Gamma_h} w^h \cdot h^h_{n+1} \quad \forall w^h \in V^h_u \quad \forall q^h \in V^h_p . \tag{23}$$

REMARK 3. The parameter θ is the one used in the θ-scheme [3]; we set it to $\frac{1}{3}$.

REMARK 4. Unlike the T6 algorithm described in [2], we add the SUPG supplement in all stages involving the advection term, i.e., in (18), (21) and (22).

REMARK 5. The matrix forms corresponding to (18), (20), (21) and (22) can be solved implicitly or explicitly as described in [2]. The matrix form of the two 'Stokes sub-steps', i.e. (19) and (23), are quite similar to the matrix form of the T1 formulation; they can be solved implicitly or by treating the velocity explicitly. The results presented in this paper are based on the explicit treatment of all sub-steps.

4. The velocity–pressure elements used

The velocity–pressure elements used in this paper are shown in Fig. 1. We now describe each element briefly.

Q1P0. This element employs bilinear interpolation for velocity and constant interpolation for pressure. It does not satisfy the Babuška–Brezzi condition and is known to suffer from spurious pressure modes. Nevertheless it is a popular element.

Q2P1. This element employs biquadratic interpolation for velocity and linear interpolation for pressure.

pQ2P1. This is the 'pseudo' version of the Q2P1 element in which the velocity is bilinear over each sub-element. In Fig. 1 these sub-elements are denoted by dashed lines.

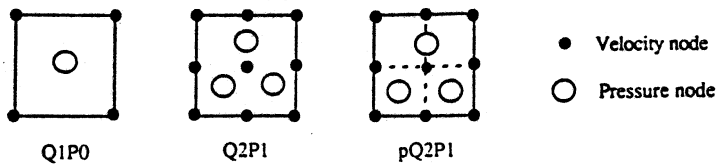

Fig. 1. The velocity–pressure elements used.

5. Numerical tests and observations

All computations were performed on the Minnesota Supercomputer Institute Cray X-MP (4 CPUs, 16 Megawords of memory, 9.5 ns clock, and UNICOS 5.0 operating system). The codes are vectorized wherever possible. To have a better basis of comparison between the solutions obtained by using different elements, we require that for each problem meshes generated with different elements have the same distribution of the velocity nodes. The nodal values of the pressure, stream function and vorticity are obtained by the least-squares interpolation.

The standing vortex problem

This test problem was suggested to us by Gresho (see [4]). The purpose of the test is to get an indication of how much numerical dissipation a formulation introduces. The flow is inviscid and is contained in a 1×1 box. The initial condition consists of an axisymmetric velocity profile with zero radial velocity, and with the circumferential velocity given as $u_\theta = \{5r$ for $r < 0.2$, $2 - 5r$ for $0.2 < r < 0.4$, 0 for $r > 0.4\}$. Since this initial condition is also the exact steady-state solution, the numerical formulation should preserve this 'standing' vortex as accurately as possible. The finite element mesh is uniform and contains 20×20 elements for Q1P0. For Q2P1 and pQ2P1 we use 10×10 elements. The time step size is 0.05; based on constant 'element length' of 0.05, this time step size results in a peak local Courant number of 1.0. The numbers of iteractions used in the sub-steps of the T6 formulation are $4-2-2-2-4-2$ for Q1P0 and pQ2P1, and $2-2-2-2-2-2$ for Q2P1.

Some of the solutions obtained at $t = 3$ (i.e., after 60 time steps) are shown in Figs. 2–7. Table 1 shows, for all three elements, the percentage of the vortex kinetic energy retained after 60 time steps.

REMARK 6. We repeated our tests, with a time step size of 1/10 of the original time step size, for the Galerkin implicit implementation of Q2P1 and pQ2P1; these implementations were still unstable.

REMARK 7. When we compare the results obtained with the T1 implicit and T1 explicit implementations of the elements considered, we see very little difference.

REMARK 8. Clearly the T6 formulation is less dissipative than the T1 formulation. Although with the T6 formulation all elements seem to yield comparable levels of dissipation, with the T1 formulation the Q1P0 element shows significantly higher dissipation. Moreover we observe that for higher-order elements the difference in energy dissipation between the T1 and T6 formulations is not as large as it is for the Q1P0 element.

REMARK 9. We repeated our tests, with a time step size of 1/3 of the original time step size, for the T1 explicit implementation of all three elements. In each case the change (compared to computations with the original time step size) in the vortex kinetic energy retained was less than 0.4%.

A related test problem, in which the initial condition consists of the superposition of a

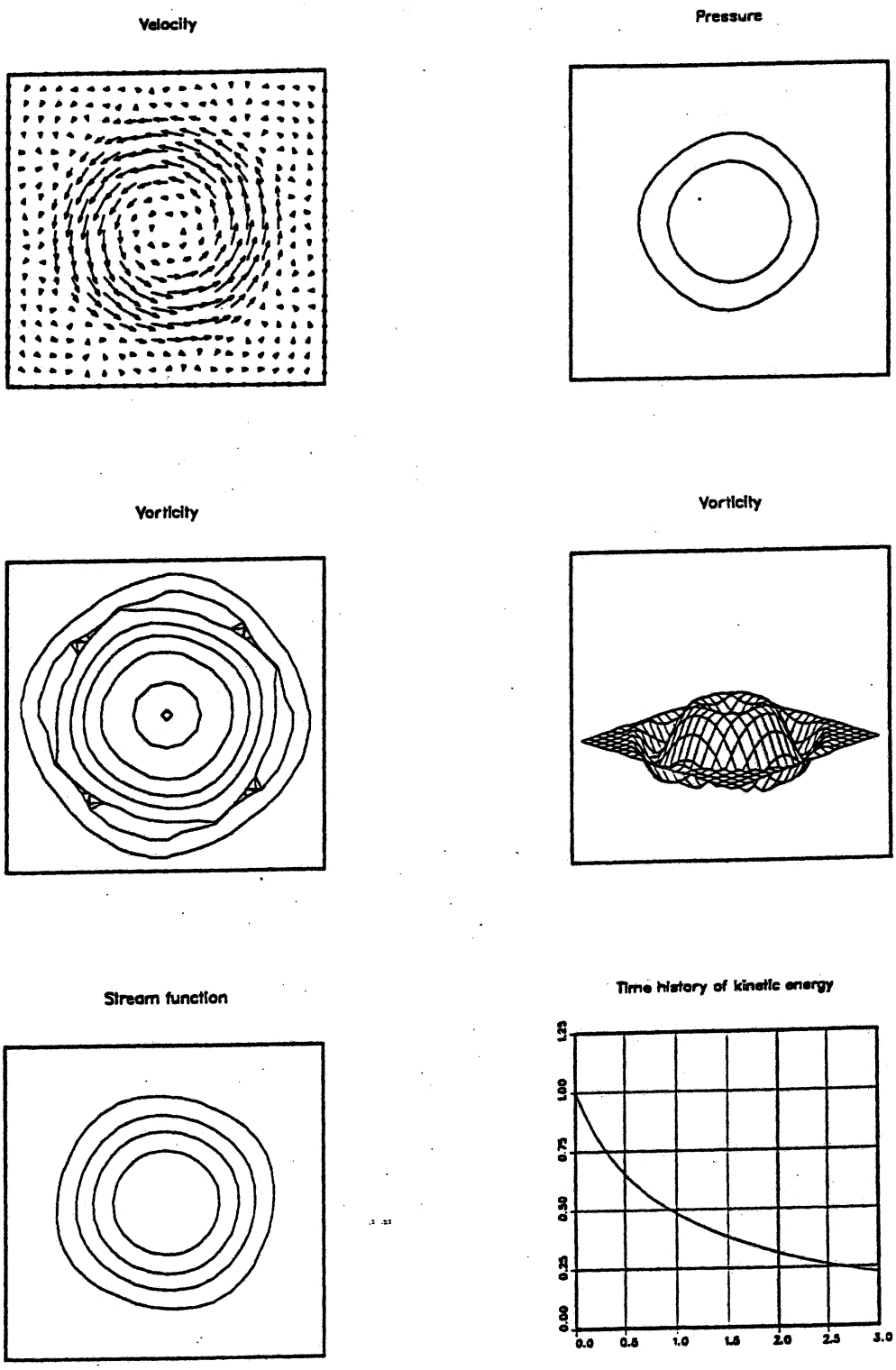

Fig. 2. Solution of the standing vortex problem at $t = 3$ with Q1P0/T1.

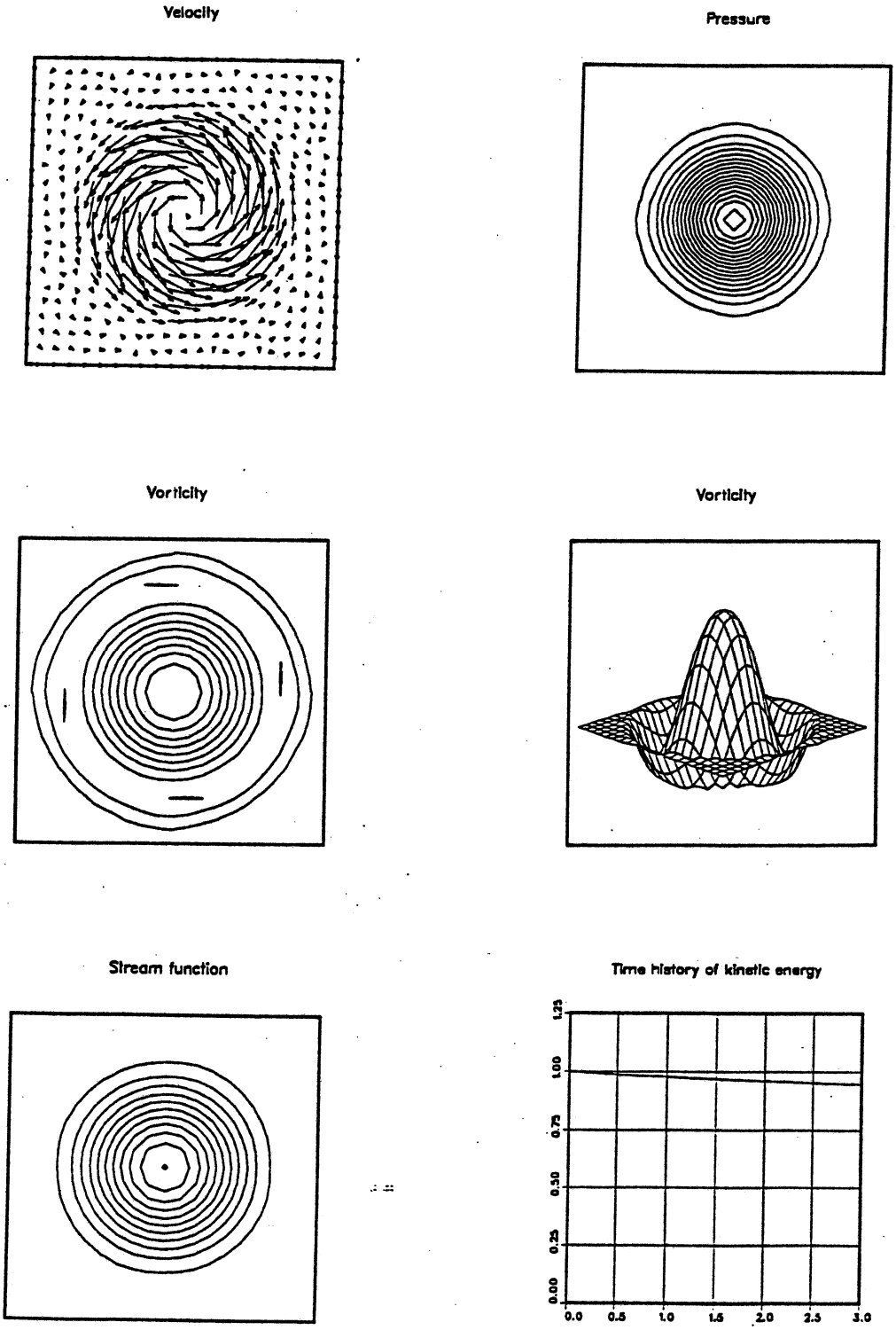

Fig. 3. Solution of the standing vortex problem at $t = 3$ with Q1P0/T6.

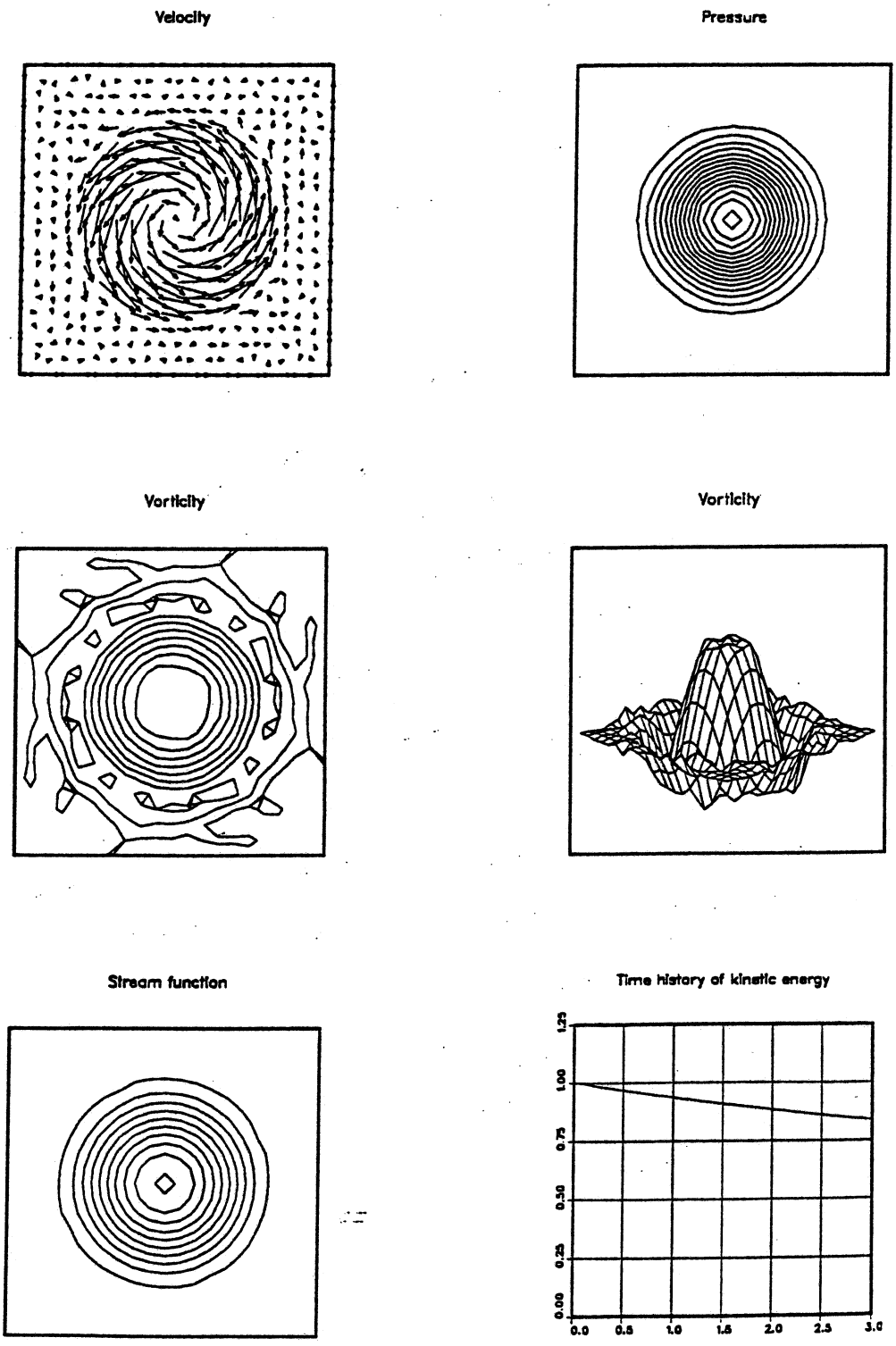

Fig. 4. Solution of the standing vortex problem at $t = 3$ with Q2P1/T1.

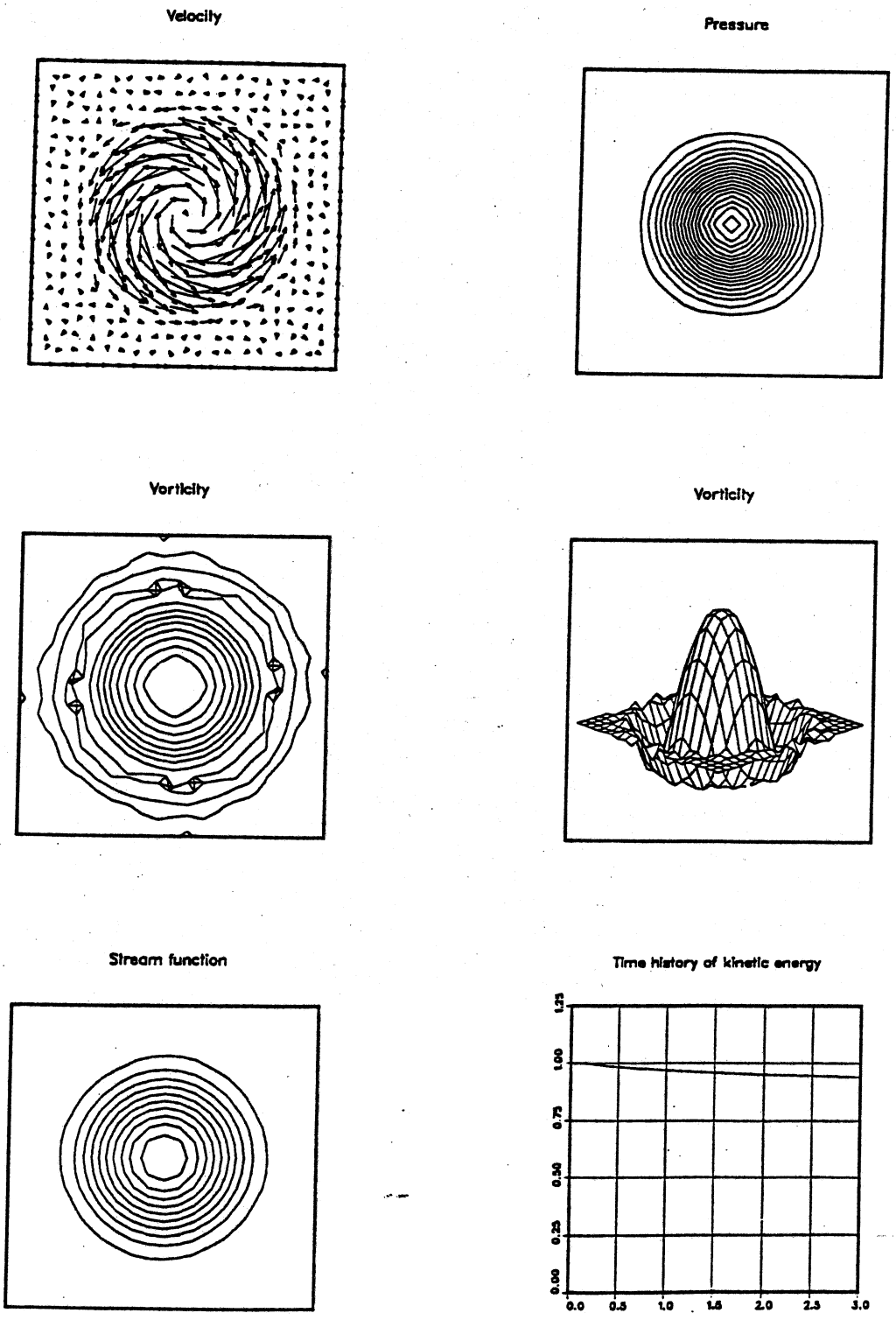

Fig. 5. Solution of the standing vortex problem at $t = 3$ with Q2P1/T6.

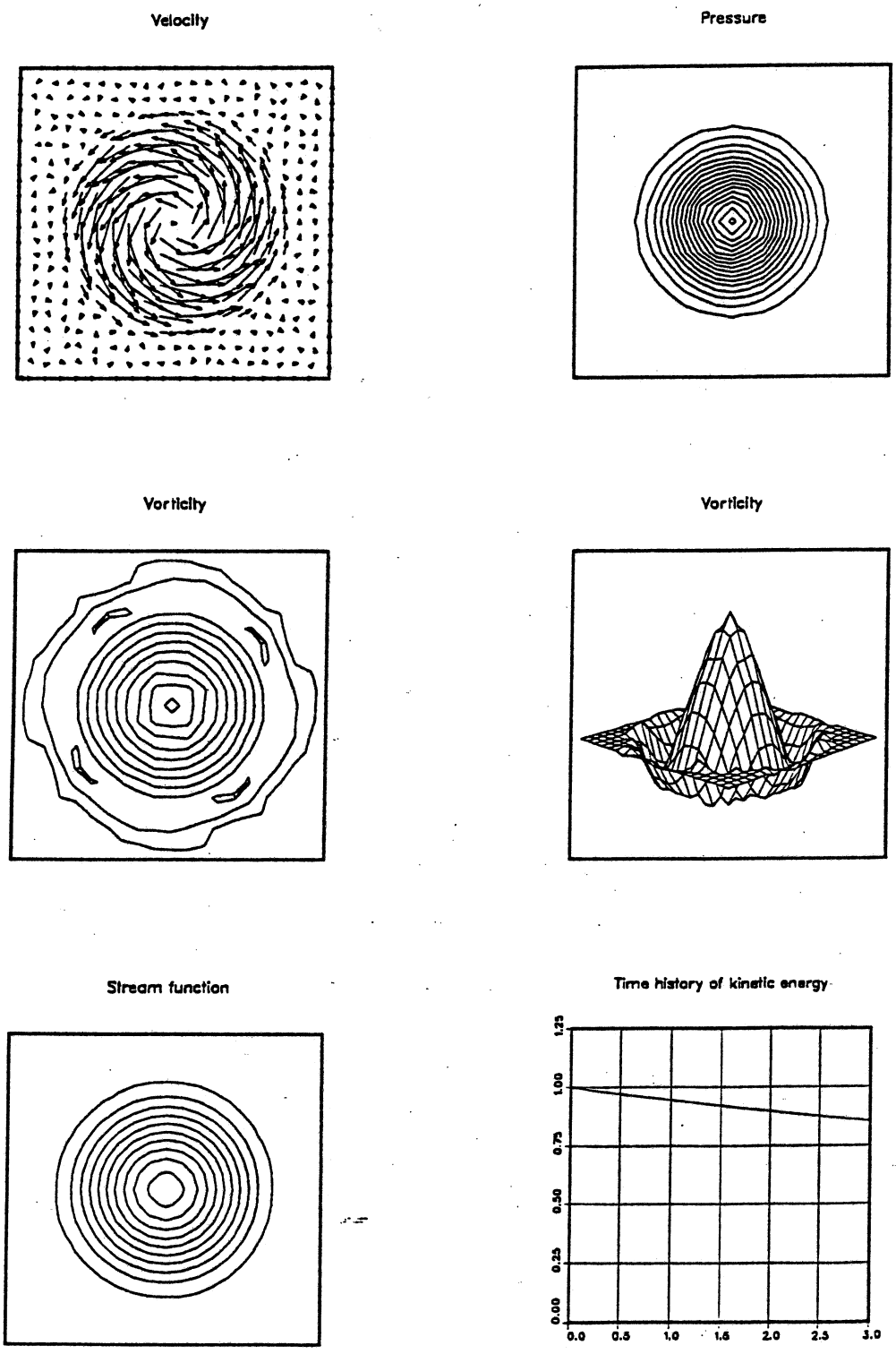

Fig. 6. Solution of the standing vortex problem at $t = 3$ with pQ2P1/T1.

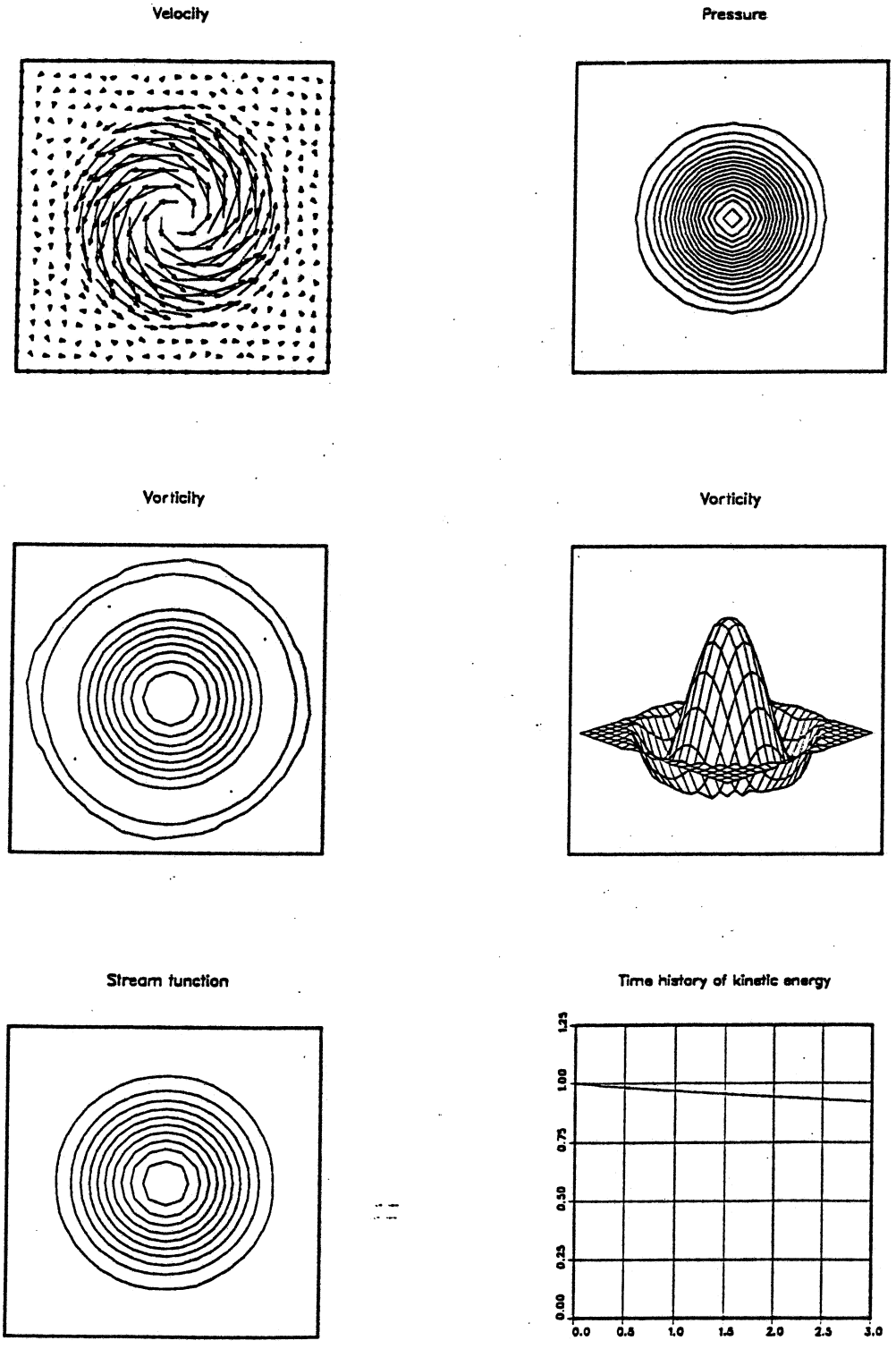

Fig. 7. Solution of the standing vortex problem at $t = 3$ with pQ2P1/T6.

Table 1

Element	Galerkin implicit	T1 implicit	T1 explicit	T6 explicit
Q1P0	100.2[a]	22.5	22.5	94.7
Q2P1	Unstable	83.7[b]	83.8[b]	94.0
pQ2P1	Unstable	85.4	85.4	92.0

[a]Strictly speaking unstable, yet the solution looks quite reasonable, except for slight oscillations that grow slowly as the computation is continued beyond $t = 3$.
[b]Slight oscillations that do not grow as the computation is continued beyond $t = 3$.

uniform flow field and the standing vortex, was considered in [4]. The boundary conditions are assumed to be consistent with the uniform flow field. It can be shown that the solution for this 'traveling vortex' is the superposition of the uniform flow field and the standing vortex translating with the velocity of the uniform flow. The proof follows.

The standing vortex flow field $u_S(\bar{x})$, $p_S(\bar{x})$ satisfies the equations

$$u_S(\bar{x}) \cdot \bar{\nabla} u_S(\bar{x}) + \frac{1}{\rho} \bar{\nabla} p_S(\bar{x}) = 0 , \tag{24}$$

$$\bar{\nabla} \cdot u_S(\bar{x}) = 0 , \tag{25}$$

where $\bar{x}$ is a generalized coordinate. The initial condition for the 'traveling vortex' is

$$u(x, 0) = u_0 + u_S(x) , \tag{26}$$

where u_0 represents a uniform flow field consistent with the boundary conditions. We need to verify that the flow field

$$u(x, t) = u_0 + u_S(x - u_0 t) , \tag{27}$$

$$p(x, t) = p_0 + p_S(x - u_0 t) , \tag{28}$$

satisfies the inviscid flow equations

$$\frac{\partial u}{\partial t} + u \cdot \nabla u + \frac{1}{\rho} \nabla p = 0 , \tag{29}$$

$$\nabla \cdot u = 0 . \tag{30}$$

Substituting (27) and (28) into the left-hand-side (LHS) of (29) and (30), we obtain

$$\text{LHS of (29)} = \frac{\partial}{\partial t} [u_0 + u_S(x - u_0 t)] + \frac{1}{\rho} \nabla [p_0 + p_S(x - u_0 t)] + [u_0 + u_S(x - u_0 t)] \cdot \nabla [u_0 + u_S(x - u_0 t)] , \tag{31}$$

$$\text{LHS of (30)} = \nabla \cdot [u_0 + u_s(x - u_0 t)] . \tag{32}$$

Recognizing $x - u_0 t$ as $\bar{x}$, and using the relations

$$\frac{\partial}{\partial t} u_s(x - u_0 t) = -u_0 \cdot \bar{\nabla} u_s(x - u_0 t) , \tag{33}$$

$$\nabla u_s(x - u_0 t) = \bar{\nabla} u_s(x - u_0 t) , \tag{34}$$

$$\nabla \cdot u_s(x - u_0 t) = \bar{\nabla} \cdot u_s(x - u_0 t) , \tag{35}$$

we arrive at

$$\text{LHS of (29)} = u_s(x - u_0 t) \cdot \bar{\nabla} u_s(x - u_0 t) + \frac{1}{\rho} \bar{\nabla} p_s(x - u_0 t) , \tag{36}$$

$$\text{LHS of (30)} = \bar{\nabla} \cdot u_s(x - u_0 t) . \tag{37}$$

By comparing (36) and (37) respectively with (24) and (25), we conclude that (27) and (28) represent a legitimate solution of (29) and (30).

Flow past a circular cylinder

In this problem we have a uniform upstream flow; the Reynolds number based on the cylinder diameter is 100. The dimensions of the computational domain, normalized by the cylinder diameter, are 30.5 and 16.0 in the flow and cross-flow directions, respectively. The mesh used for Q1P0 consists of 5240 elements, while the number of elements for Q2P1 and pQ2P1 is 1310. All meshes contain 5350 velocity nodes. The numbers of iterations used in the sub-steps of the T6 formulation are 4 – 2 – 2 – 2 – 4 – 2 for Q1P0 and pQ2P1, and 2 – 2 – 2 – 2 – 2 – 2 for Q2P1. In each case, the CPU time (in seconds) per time step is 0.51 (Q1P0/T1), 1.10 (Q1P0/T6), 0.64 (Q2P1/T1), 0.83 (Q2P1/T6), 0.57 (pQ2P1/T1), 0.86 (pQ2P1/T6). For each element, to expedite the convergence to the temporally periodic solution, as initial condition we use the solution corresponding to the crest value of the lift coefficient obtained with Q2P1/T6. The periodic solution for Q2P1/T6 is computed by introducing a short term perturbation to the symmetric solution obtained with this formulation. We have observed, at least for small perturbations, that the periodic solution is independent of the mode of perturbation.

The Strouhal number and the time history of the lift and drag coefficients are shown in Figs. 8 and 9. For all formulations except for Q1P0/T1, which results in a significantly lower value, the variations in the Strouhal number is within 2% range. The lift coefficient shows no significant difference among different formulations except Q1P0/T1. For the drag coefficient, the values obtained with Q1P0/T6, Q2P1/T6, pQ2P1/T6 and Q2P1/T1 are very close, while the value obtained with pQ2P1/T1 is lower, and the value obtained with Q1P0/T1 is significantly lower.

The periodic flow patterns corresponding to the crest value of the lift coefficient are shown in Figs. 10–15. The patterns corresponding to the trough value of the lift coefficient are simply

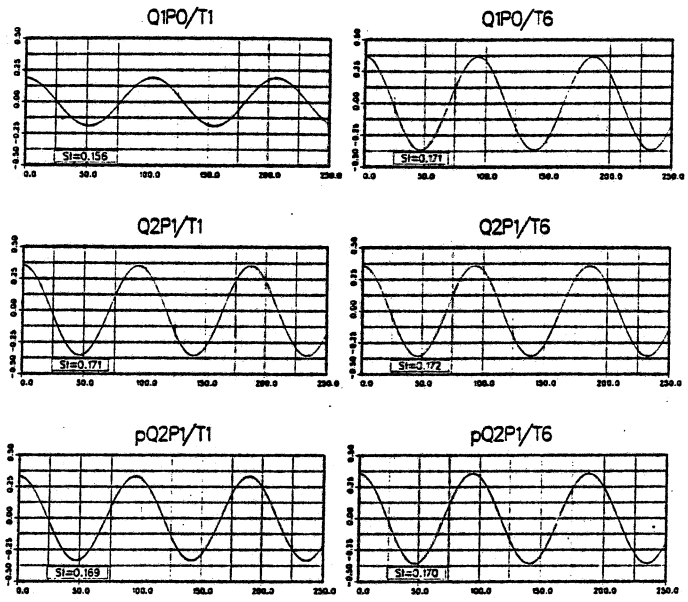

Fig. 8. The Strouhal number and the time history of the lift coefficient obtained with various elements.

the mirror images, with respect to the horizontal centerline of the patterns shown in Figs. 10–15. We observe that the solutions obtained with Q1P0/T6 and pQ2P1/T6 are very similar, and the solutions obtained with Q2P1/T1 and Q2P1/T6 are very similar. It is clear from all these flow patterns that the T6 formulation is less dissipative than the T1 formulation. This observation is the same as the one we made for the standing vortex problem. For Q2P1,

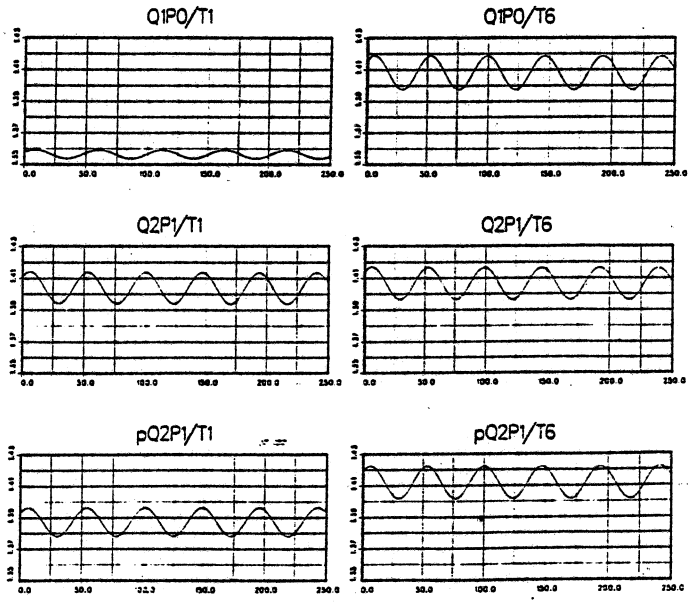

Fig. 9. The time history of the drag coefficient obtained with various elements.

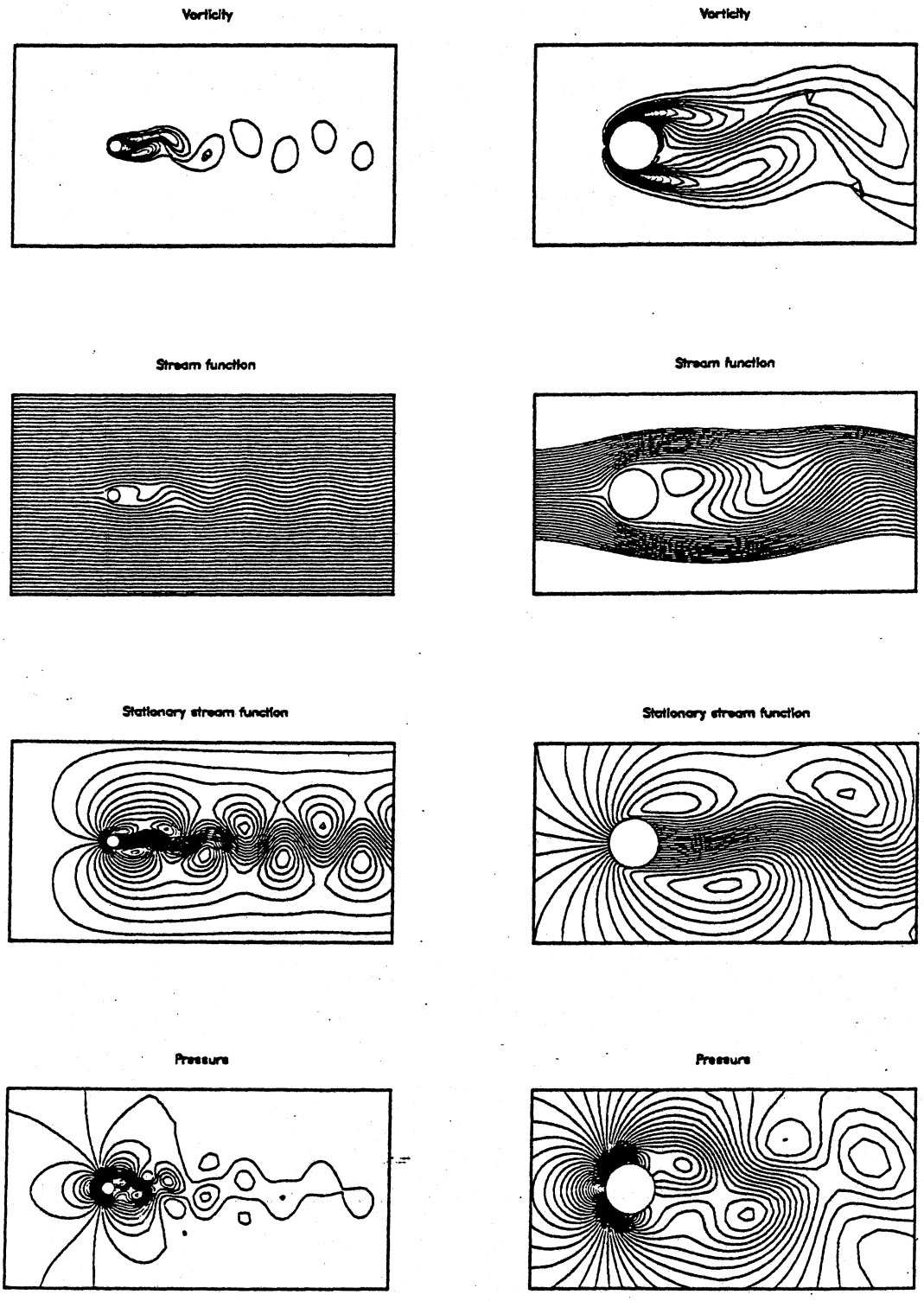

Fig. 10. Periodic solution (corresponding to the crest value of the lift coefficient) obtained with Q1P0/T1.

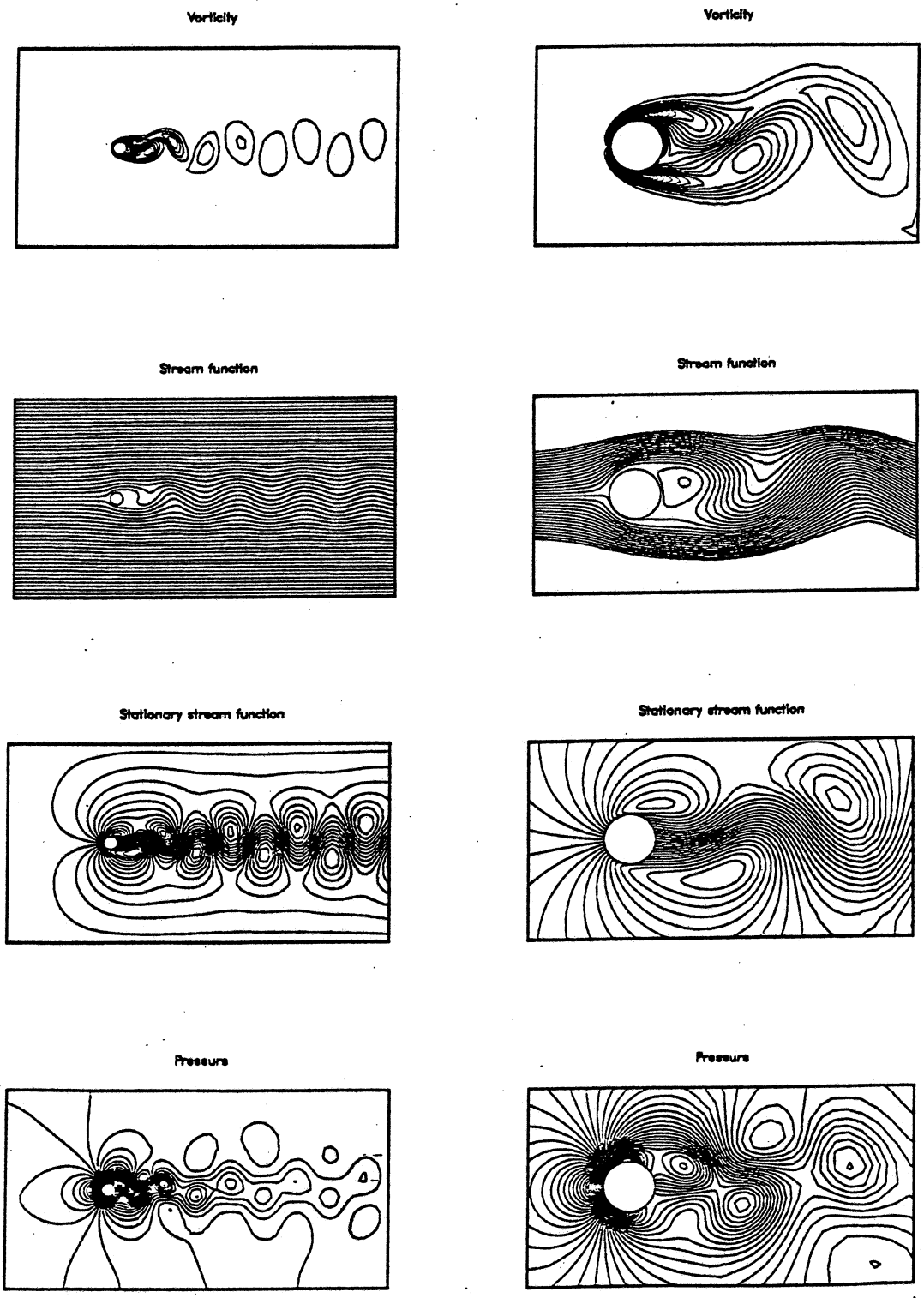

Fig. 11. Periodic solution (corresponding to the crest value of the lift coefficient) obtained with Q1P0/T6.

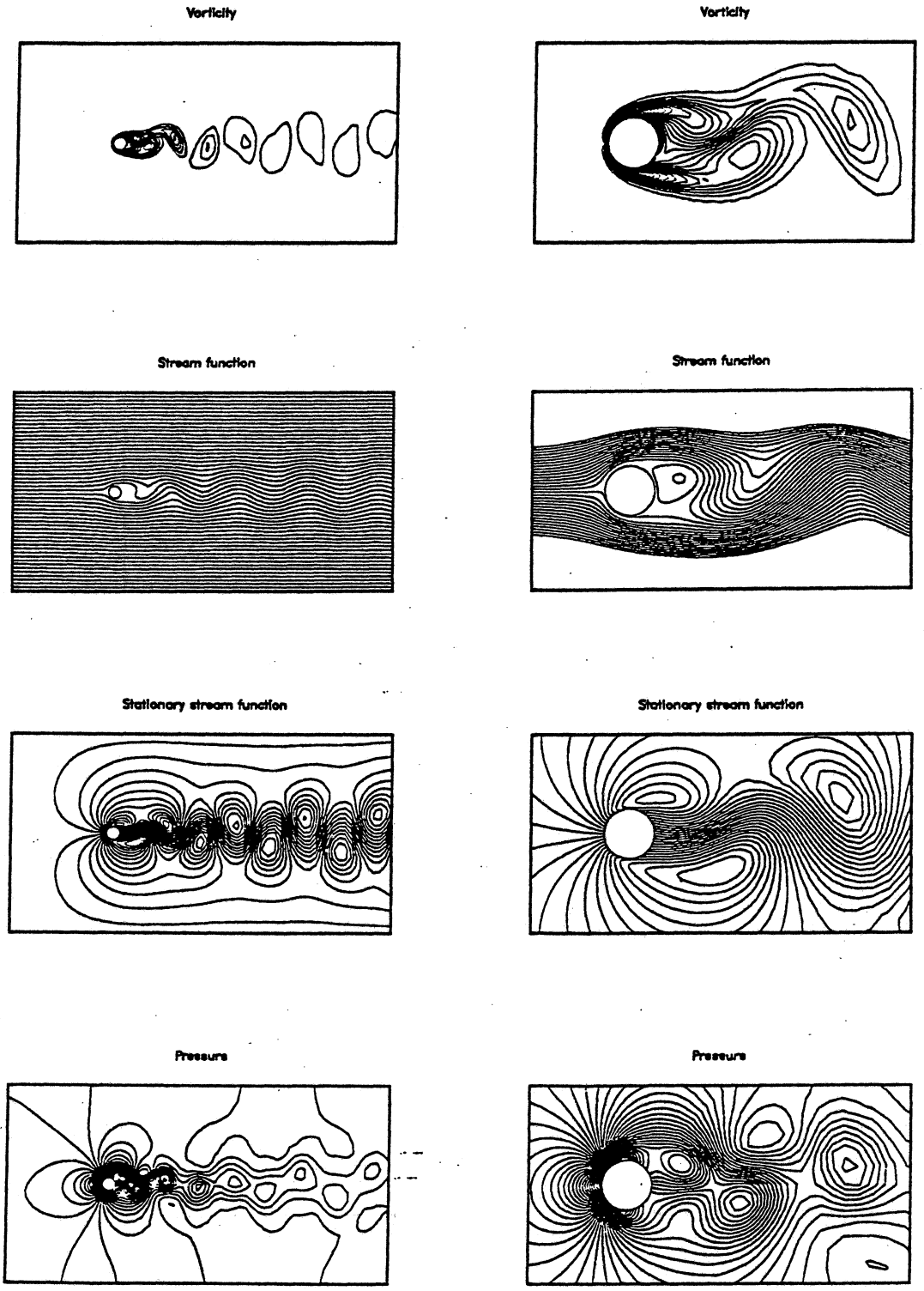

Fig. 12. Periodic solution (corresponding to the crest value of the lift coefficient) obtained with Q2P1/T1.

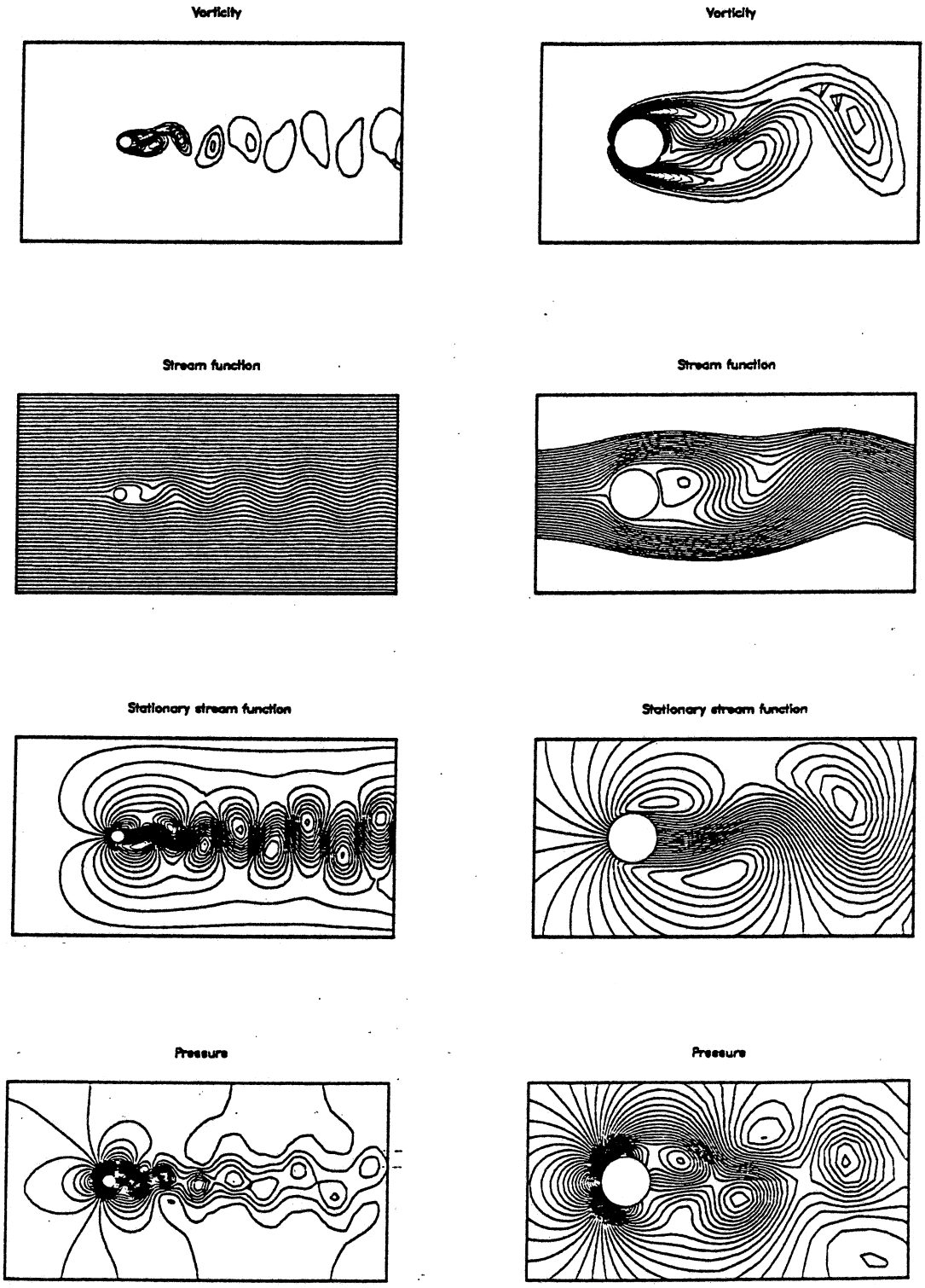

Fig. 13. Periodic solution (corresponding to the crest value of the lift coefficient) obtained with Q2P1 T6.

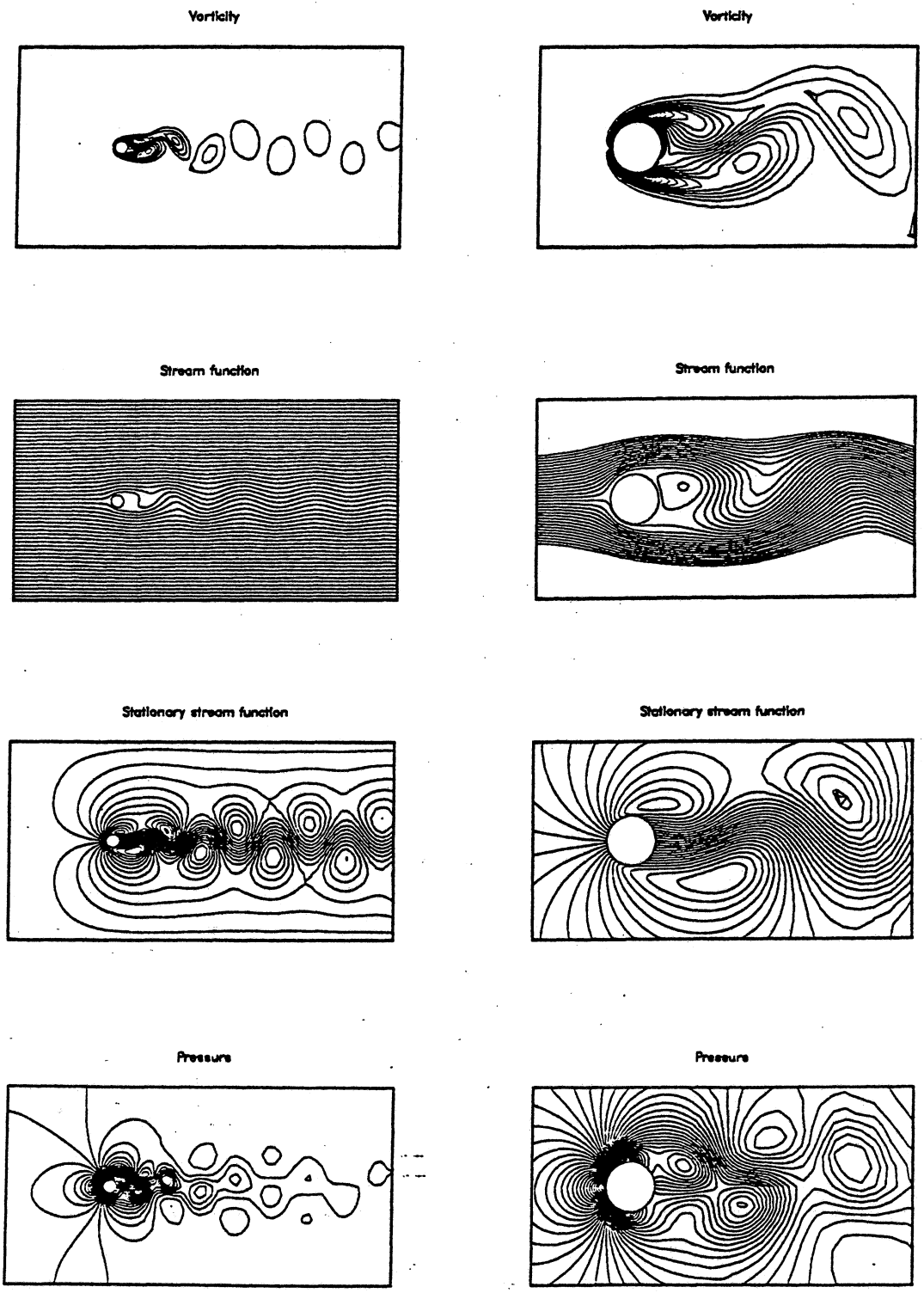

Fig. 14. Periodic solution (corresponding to the crest value of the lift coefficient) obtained with pQ2P1/T1.

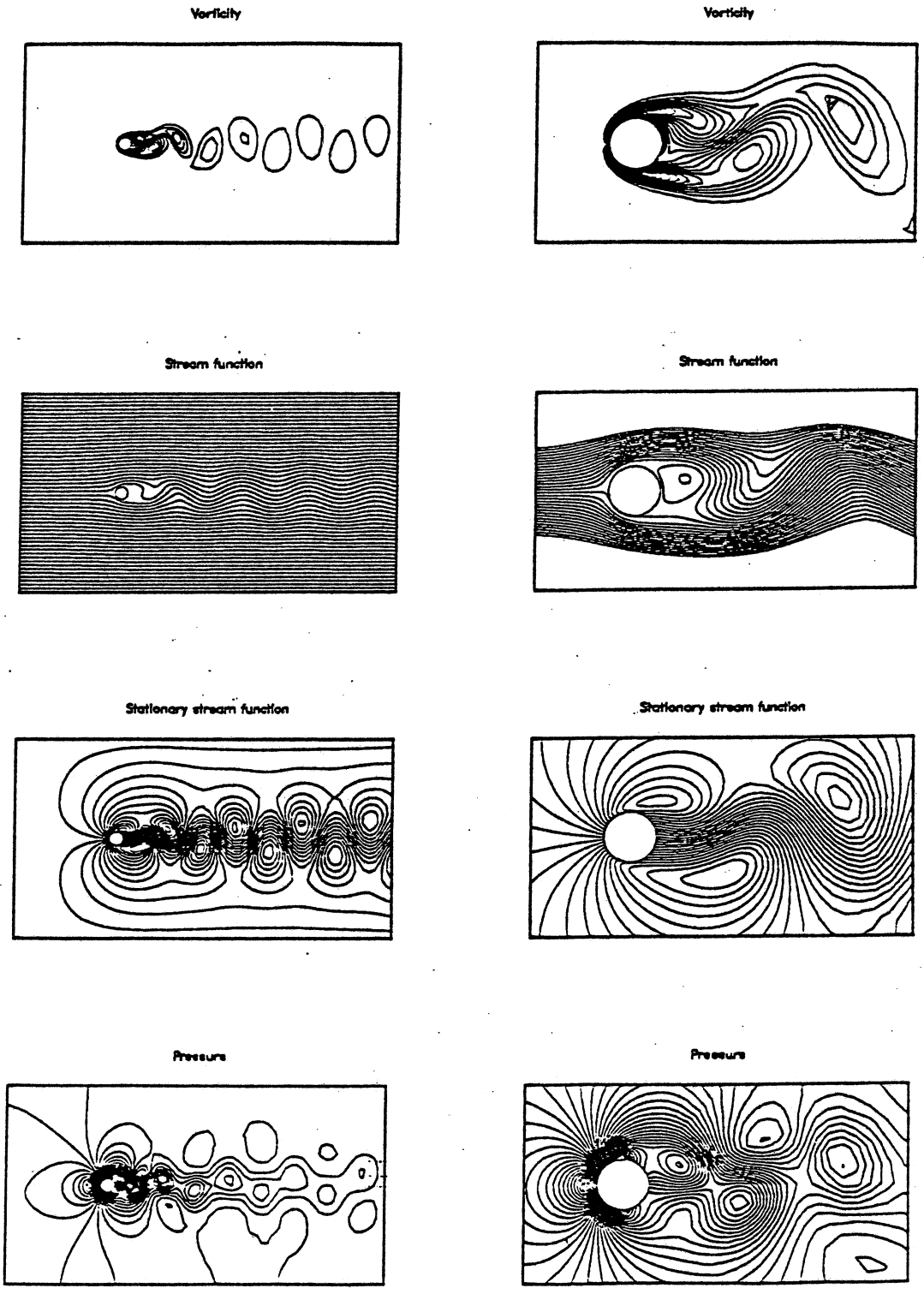

Fig. 15. Periodic solution (corresponding to the crest value of the lift coefficient) obtained with pQ2P1. T6.

however, the difference between the patterns obtained with the T1 and T6 formulations is not significant.

We repeated our computations, with a time step size of 1/3 the original time step size, for the T1 implementation of all elements; there was no significant change in the solutions obtained.

6. Concluding remarks

We investigated, in the context of time-accurate finite element computation of unsteady incompressible flows, the performance of the quadrilateral velocity–pressure elements with constant and linear pressure interpolations. These elements were implemented using the one-step (T1) and six-step (T6) formulations of the Navier–Stokes equations. We picked two numerical examples: the standing vortex problem and flow past a circular cylinder. Results from these two test problems show that the T6 formulation is less dissipative than the T1 formulation. Although with the T6 formulation all elements seem to yield comparable levels of dissipation and similar solutions, with the T1 formulation the Q1P0 element shows signficantly higher dissipation.

References

[1] A.N. Brooks and T.J.R. Hughes, Streamline upwind/Petrov–Galerkin formulations for convection dominated flows with particular emphasis on the incompressible Navier–Stokes Equation, Comput. Methods Appl. Mech. Engrg. 32 (1982) 199–259.

[2] T.E. Tezduyar, J. Liou and D.K. Ganjoo, Incompressible flow computations based on the vorticity–stream function and velocity–pressure formulations, Comput. & Structures 35 (1990) 445–472.

[3] M.O. Bristeau, R. Glowinski and J. Periaux, Numerical methods for the Navier Stokes equations: Applications to the simulation of compressible and incompressible viscous flows, Comput. Phys. Rep. 6 (1987) 73–187.

[4] P.M. Gresho and S.T. Chan, Semi-consistent mass matrix techniques for solving the incompressible Navier–Stokes equations, Lawrence Livermore National Laboratory, Preprint UCRL-99503, 1988.

[5] M. Braza, P. Chassaing and H.H. Minh, Numerical study and physical analysis of the pressure and velocity fields in the near wake of a circular cylinder, J. Fluid Mech. 165 (1986) 79–130.

[6] J.H. Gerrard, The wakes of cylindrical bluff bodies at low Reynolds number, Philos. Trans. Roy. Soc. London Ser. A 288 (1978) 351–382.

[7] M.S. Engelman and M. Jamnia, Transient flow past a circular cylinder, Internat. J. Numer. Methods Fluids (1990) to appear.

[8] T.E. Tezduyar, J. Liou, D.K. Ganjoo and M. Behr, Unsteady incompressible flow computations with the finite element method, (Hemisphere, Washington) to appear.